Supporting Information

# La-modified nanocrystalline $Cu_4(NO_3)_2(OH)_6$ for highly selective $CO_2$ reduction into $CH_4$ under near-infrared light illumination

Jia Wang[a], Yue Liu[a,b,*], Yuancheng Peng[a], Peng Xie[a], Pengjun Wu[a], Lihai Zhou[a], Binbing Tang[c], Mingpeng Zhuo[d,*], Xinyu Ding[f], Xiaolei Yuan[f], and Weifan Chen[a,b,e,*]

[a] School of Physics and Materials Science, Nanchang University, Nanchang, Jiangxi 330031, P. R. China.

[b] Institute of Rare Earths, Nanchang University, Nanchang, Jiangxi 330031, P. R. China.

[c] Institute for Advanced Study, Nanchang University, Nanchang, Jiangxi 330031, P. R. China.

[d] National Engineering Laboratory for Modern Silk, College of Textile and Clothing Engineering, Soochow University, Suzhou, Jiangsu 215123, P. R. China.

[e] Jiangxi Sun-Nano Advanced Materials Technology Co. Ltd, Ganzhou, Jiangxi 341000, P. R. China.

[f] School of Chemistry and Chemical Engineering, Nantong University, Nantong, Jiangsu 226019, P. R. China.

* Corresponding authors

Authors to whom correspondence should be addressed: chenweifan@ncu.edu.cn (W. F. Chen).

**Materials**

Copper nitrate trihydrate ($Cu(NO_3)_2 \cdot 3H_2O$), Lanthanum acetate trihydrate ($C_6H_9LaO_6 \cdot 1.5H_2O$), All reagents were of analytical grade and used without further purification.

**Synthesis of CuNH and La/CuNH**

The precursor $Mg(OH)_2$ nanoflowers was prepared according to our previous work [1]. The $Cu(NO_3)_2$ solution was obtained by dissolving 24.22 g $Cu(NO_3)_2 \cdot 3H_2O$ into 50 mL deionized water. Then, 3 g $Mg(OH)_2$ precursor was dispersed in 50 mL deionized water, and the above $Cu(NO_3)_2$ solution was slowly dropped in the dispersion under magnetic stirring. After vigorous stirring for 2 h, the mixture was aged at room temperature for about 7 h. The powder was collected by centrifugation, washed with deionized water and ethanol for several times, and then dried at 60℃ for 12 h. Subsequently, 1 g of the above prepared powder and different amounts of $C_6H_9LaO_6 \cdot 1.5H_2O$ were mixed and ground in an agate mortar for 1 h to achieve a mechanochemical reaction. La/CuNH can be obtained by washing the mixture with deionized water and drying. The contents of La in La/CuNH are shown in Tables S1 and S2. For comparison, CuNH was synthesized by the same process except for the absence of $C_6H_9LaO_6 \cdot 1.5H_2O$.

**Sample preparation for measurements**

For powder-based measurements (XRD, XPS, EPR, DRS, PL and water angle tests), the samples were directly measured without further treatment. For SEM, the samples were fixed on the sample stage with conductive adhesive tape, followed by

spray-gold treatment. For TEM, the sample was dispersed in ethanol, dropped onto a copper grid, and dried naturally. For ICP, the samples were dissolved in nitric acid and then diluted to a specified volume. For FTIR, each sample was thoroughly ground with NaCl and pressed into a pellet. To prepare a working electrode for photoelectrochemical measurements, 10 mg sample was dispersed in 1 mL ethanol and 50 μL Nafion solution, and sonicated for 30 min. Then 100 μL of the dispersion was dropped on an ITO glass (2 cm × 2 cm), the dried sample coated on glass was served as a working electrode. For in situ FT-IR, the samples were purged with Ar in the dark for 30 min.

**Characterization**

The X-ray powder diffraction (XRD) patterns were recorded by a SmartLab 9KW instrument. Scanning electron microscopy (SEM) images were captured by a microscope (ZEISS/Sigma 560, Carl Zeiss Microscopy). The micromorphology and diffraction spot were investigated by transmission electron microscope (TEM, JEM-F200, JEOL) with selected area electron diffraction (SAED). The content of La in La/CuNH was quantified by an inductively coupled plasma mass spectrometry (ICP-MS, iCAP-RQ, Thermo Fisher Scientific). Fourier transform infrared spectroscopy (FTIR) was performed to characterize chemical bonds of materials on a spectrometer (ALPHA, Bruker). The surface element composition and chemical state of photocatalysts were analyzed by X-ray photoelectron spectroscopy (XPS, ESCALAB Xi+, Thermo Fisher Scientific). All of the binding energies were calibrated by the C 1s peak at 284.8 eV. Electron paramagnetic resonance (EPR) was performed on a spectrometer (E500-10/12, Bruker). The diffuse reflectance spectra (DRS) were

measured by a UV-visible-NIR spectrophotometer (UH-4150, HITACHI) in the wavelength range 250-2500 nm. Photoluminescence spectra were recorded using a spectrofluorometer (FLS980, Edinburgh Instruments) with 380 nm excitation wavelength. In situ FT-IR measurements were conducted using a FT-IR spectrometer (INVENIO R, Bruker) equipped with an in situ diffuse reflectance cell. Water contact angle tests were conducted by a contact angle goniometer (SDC-350H, SINDIN).

**Photocatalytic $CO_2$ reduction**

The photoreduction activity of catalysts was evaluated in a gas-solid reactor via a Labsolar-6A closed circulation system (Beijing PerfectLight). 30 mg catalyst was uniformly dispersed by ultrasound for 30 min in 10 mL deionized water. The catalyst was coated on a glass fiber filter and dried at 60℃ to form a uniform film. The prepared film was put on the top of a quartz tray. The sealed reactor was vacuumed and washed with high-purity $CO_2$ (99.999%) for several times. The pressure of $CO_2$ as a reactive gas was ultimately maintained at ~80 Kpa. 4 mL deionized water was injected under the quartz tray to ensure no direct contact with photocatalysts. Before irradiation, a balance between adsorption and desorption was established. A 300W Xe lamp (PLS-SXE300/300UV, Beijing PerfectLight) with an 800 nm cutoff filter was used as NIR light source, and the distance from the lamp to the sample was ~10 cm. The temperature of photoreactor was controlled at 5℃ by circulating cooling water. The details of the photocatalytic device were clarified by a simple model (Fig. S7). The products can be detected and analyzed by a gas chromatograph (GC, A60, PANNA) equipped with thermal conductivity detector (TCD) and flame ionization detector (FID).

**Calculation of evolution rate of $CH_4$ and CO**

According to the equation of state of ideal gas ($PV = nRT$), the evolution rate of the formed $CH_4$ and CO can be deduced and calculated by the following formula when the pressure ($P$) is one atmospheric pressure:

$$P_1 \cdot V_m^{'}/T_1 = P \cdot V_m/T$$

$$n^{'} = V^{'}/V_m^{'}$$

$$\varphi(gas) = n^{'}/(t \cdot m)$$

Where $V_m$ = 22.4 L/mol is molar volume of gas under standard conditions ($P$ = 101.325 Kpa, $T$ = 273.15 K), $V_m'$ represents the actual molar volume of gas when reaction pressure $P_1$ = 80 Kpa, reaction temperature is $T_1$ = 278.15 K, $n'$ is the amount of product gas ($CH_4$ or CO) and $V'$ is tested volume, φ(gas) represents the evolution rate of product gas ($CH_4$ or CO), $t$ is the reaction time, and $m$ is the amount of photocatalyst.

**Calculation of selectivity of $CH_4$ and CO**

The selectivity of the formed $CH_4$ and CO is calculated according to the following equation:

$$Selectivity\ for\ CH_4 = \frac{8R(CH_4)}{8R(CH_4) + 2R(CO)} \times 100\%$$

$$Selectivity\ for\ CO = \frac{2R(CO)}{8R(CH_4) + 2R(CO)} \times 100\%$$

Where R($CH_4$) and R(CO) are the yields of reactively-formed $CH_4$ and CO respectively.

**Photoelectrochemical measurements**

The photoelectrochemical (PEC) tests were conducted by a CS1350 electrochemical station with a standard three-electrode system. Pt foil and Ag/AgCl

electrode acted as the counter electrode and reference electrode, respectively. 0.5 M $Na_2SO_4$ solution was used as an electrolyte. Transient photocurrent response was measured with an applied voltage of 0.5 V. Electrochemical impedance spectroscopy (EIS) was performed by applying a sine wave with amplitude of 5 mV over the frequency range of 0.01 Hz-100 kHz. All experiments were conducted under NIR light irradiation (λ≥800 nm, PLS-SXE300/300UV, Beijing PerfectLight).

**Density Functional Theory calculations**

The theoretical study was carried out with first-principles calculations based on density functional theory. The electronic characteristics were analyzed using the Projector Augmented Wave (PAW) method, implementing the Perdew-Burke-Ernzerhof (PBE) exchange-correlation function within the framework of the Generalized Gradient Approximation (GGA). The total energies were converged to a precision of at least $2\times10^{-6}$ eV per atom using a plane wave cutoff energy of 400 eV and a Monkhorst-Pack grid of 3 × 3 × 3. The iterative convergence criterion of energy is set at $10^{-5}$ eV. A vacuum layer of 15 Å was applied to avoid interactions between periodic images. The adsorption energy was computed as follow:

$$\Delta E_{ads} = E_{system} - E_{slab} - E_{CO2/CO}$$

Where $E_{system}$, $E_{slab}$, $E_{CO2/CO}$ represent the energy of system, pure slab and $CO_2$ or CO, respectively. The free energy was computed as follow:

$$\Delta G = E_{DFT} + G_{corr}$$

$$G_{corr} = U_{0-->298.15\ K} + PV + E_{ZPE} - TS$$

Where $E_{DFT}$, $G_{corr}$ represent the electronic energy and correction energy of all system, respectively. $E_{ZPE}$ is the zero-point energy, T is 298.15 K. S is the entropy.

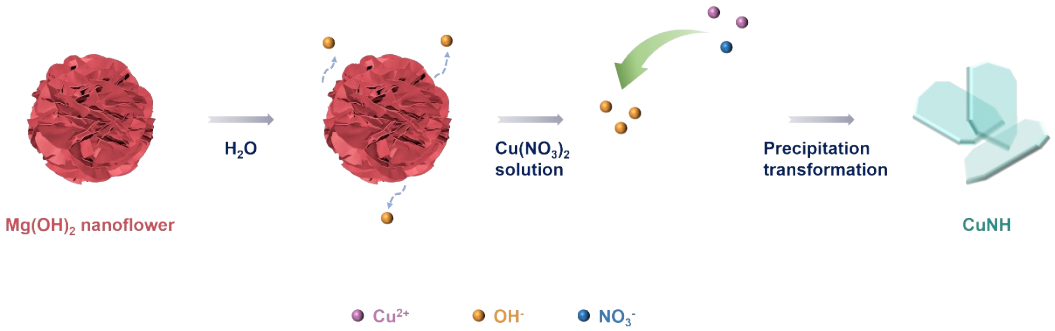


**Fig. S1.** The synthesis route of $Cu_4(NO_3)_2(OH)_6$.

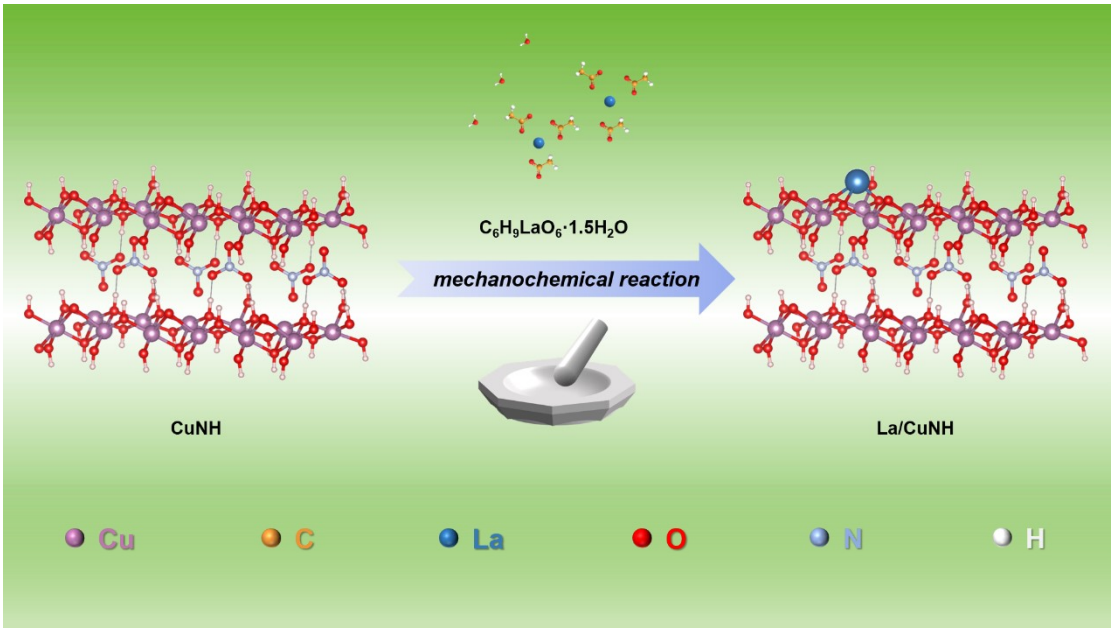


**Fig. S2.** Schematic illustration for the decoration of La on nanocrystalline $Cu_4(NO_3)_2(OH)_6$.

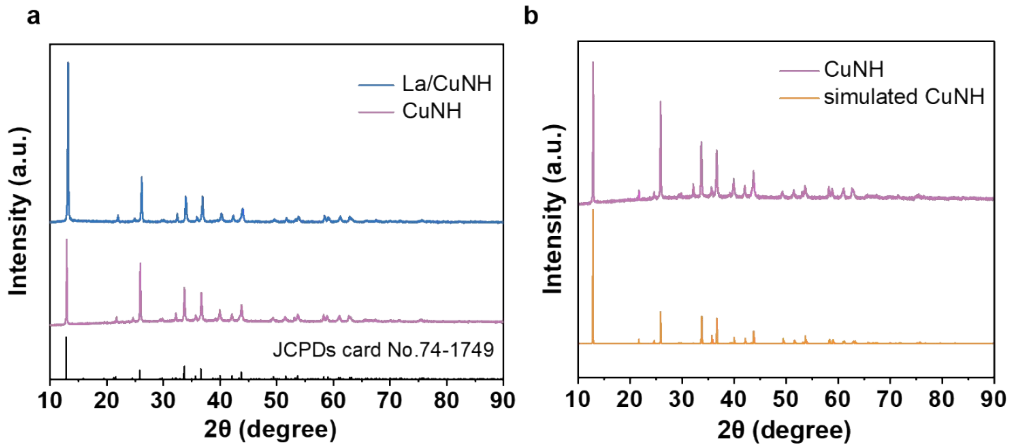


**Fig. S3.** (a) The experimental XRD patterns of CuNH and La/CuNH. (b) The comparison simulated and measured XRD patterns of CuNH.

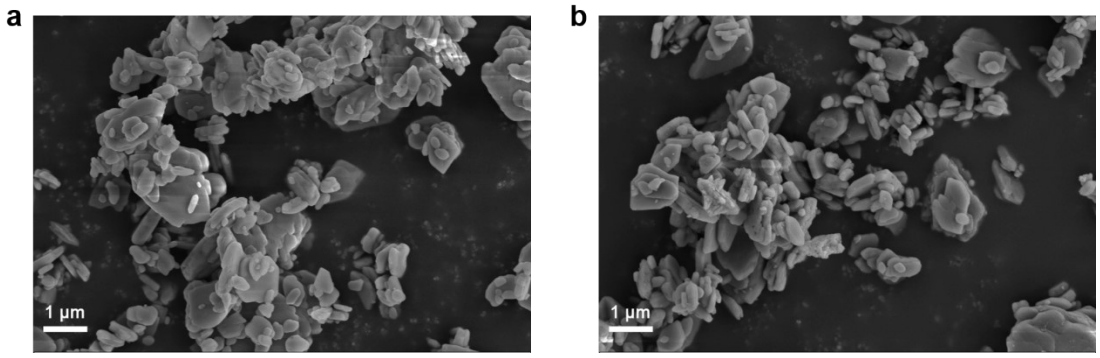


**Fig. S4.** The SEM images of (a) CuNH and (b) La/CuNH.

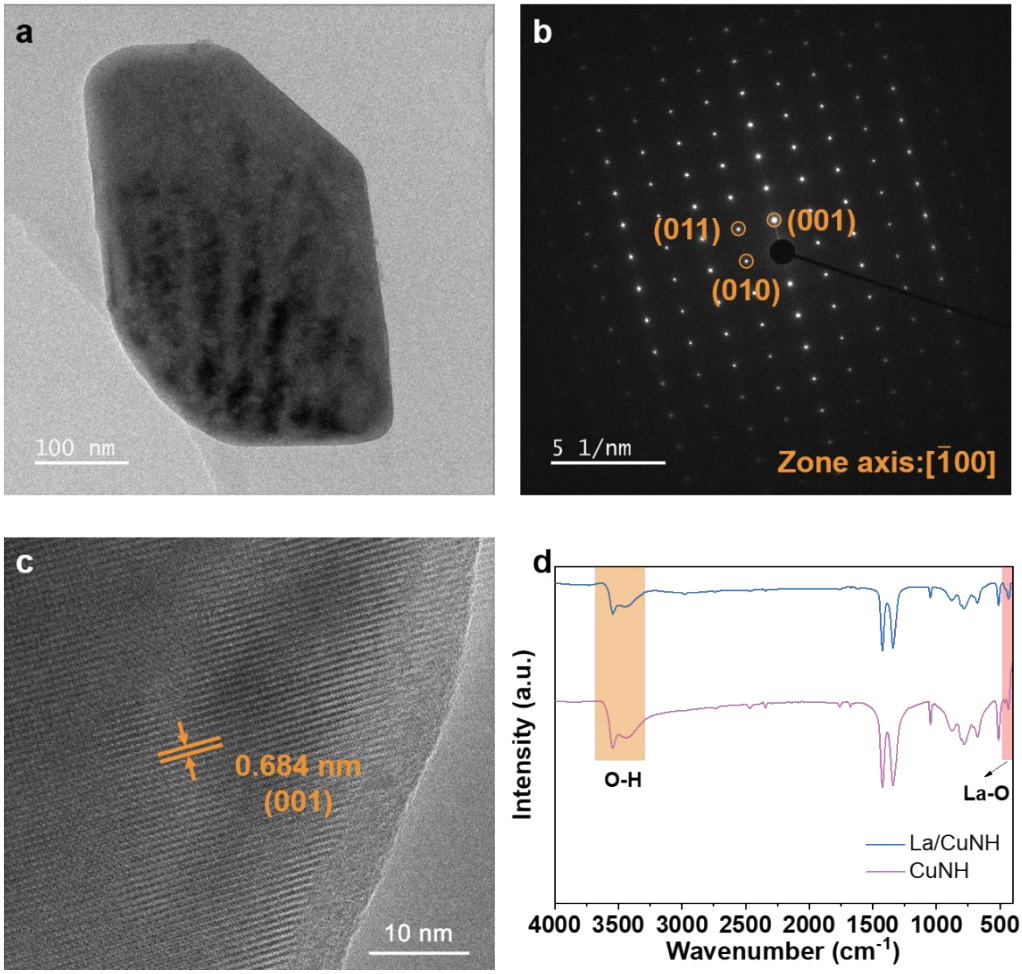


**Fig. S5.** (a) TEM image, (b)SAED pattern and (c) HRTEM image of La/CuNH. (d) FT-IR spectra of CuNH and La/CuNH.

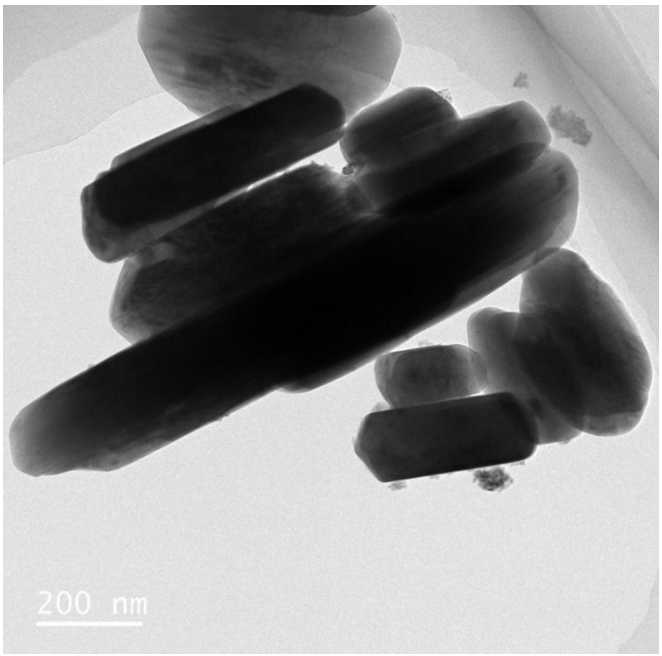


**Fig. S6.** The supplementary TEM image of La/CuNH.

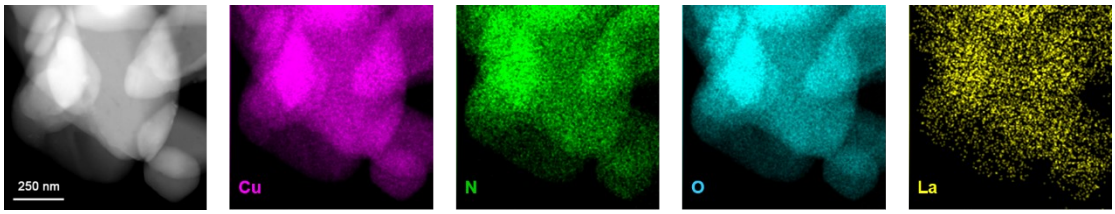


**Fig. S7.** The TEM-EDS elemental mappings of La/CuNH.

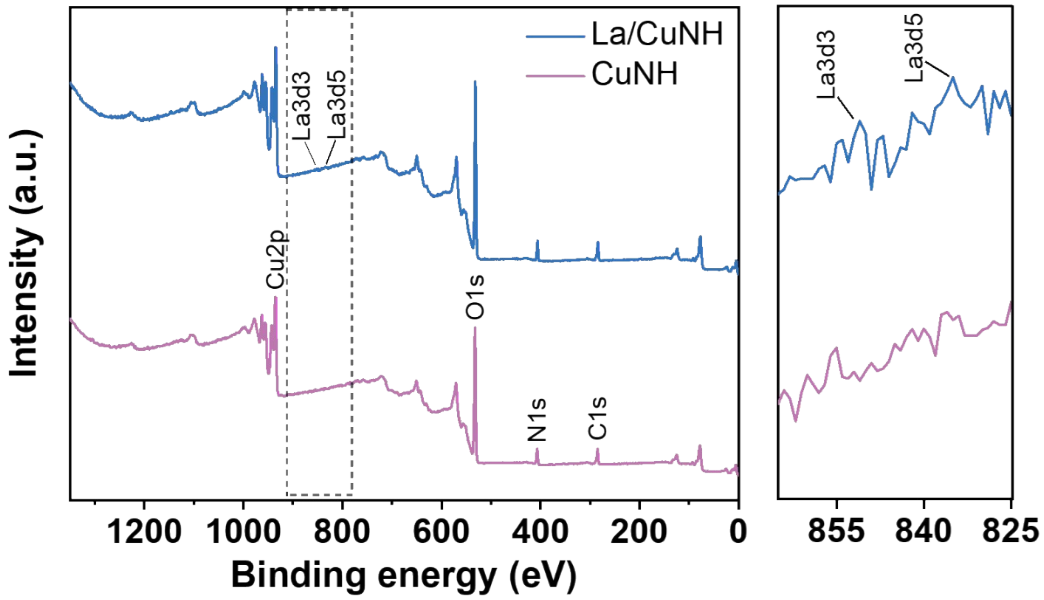


**Fig. S8.** XPS survey spectra of CuNH and La/CuNH, and the corresponding local magnification in the binding energy range of 855-825 eV.

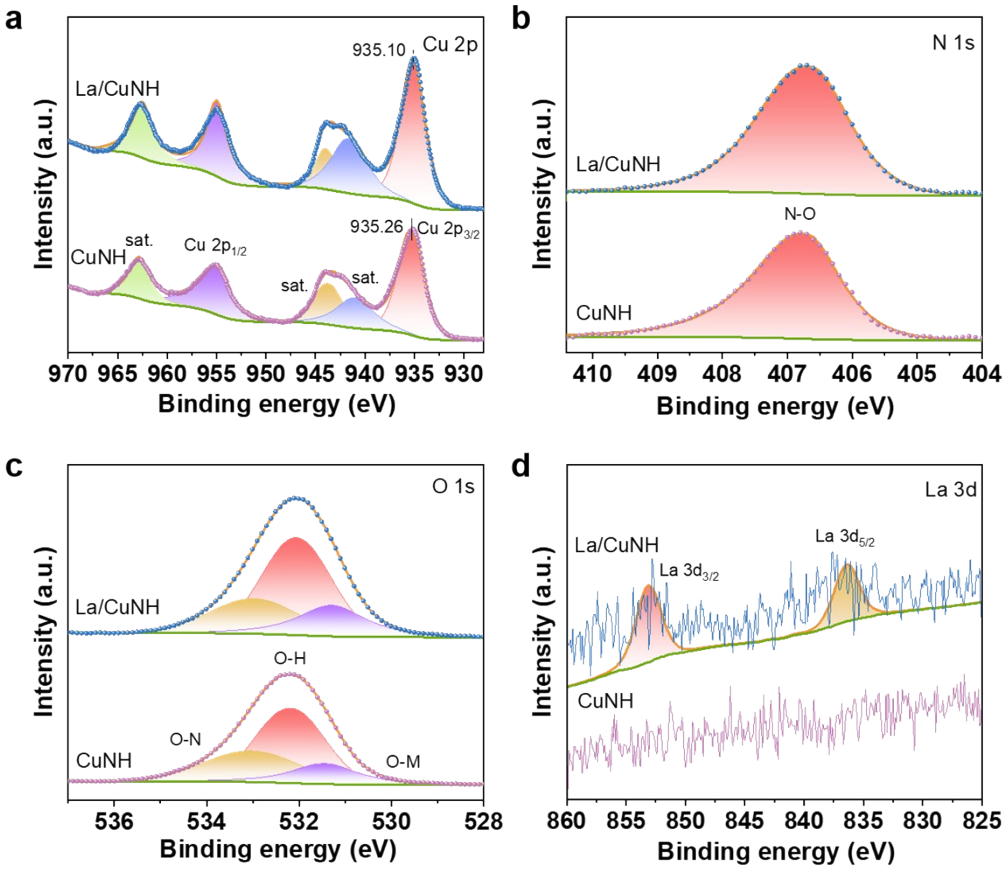


**Fig. S9.** High-resolution XPS spectra of CuNH and La/CuNH: (a) Cu 2p, (b) N 1s, (c) O 1s, and (d) La 3d.

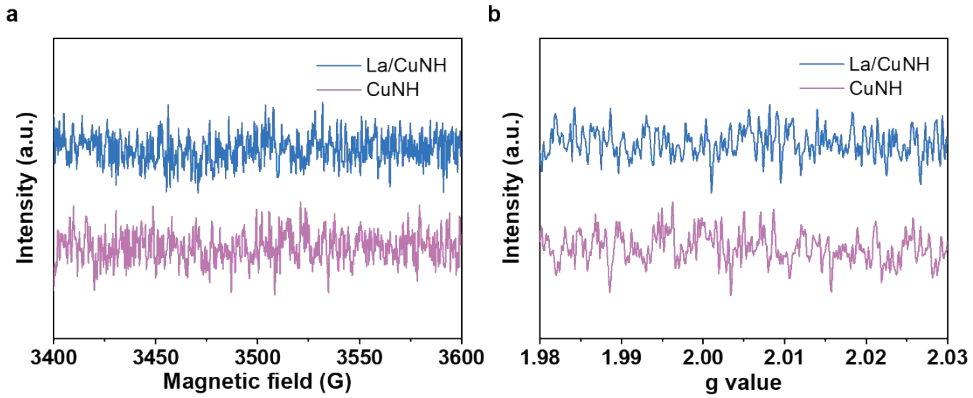


**Fig. S10.** The EPR spectra of CuNH and La/CuNH.

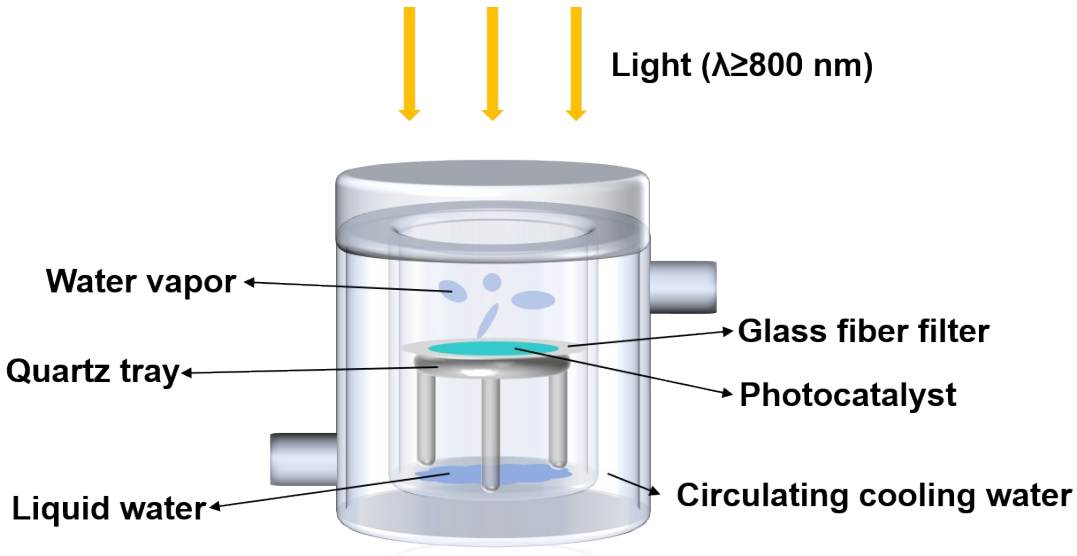


**Fig. S11.** The schematic diagram of photocatalytic gas-phase reactor.

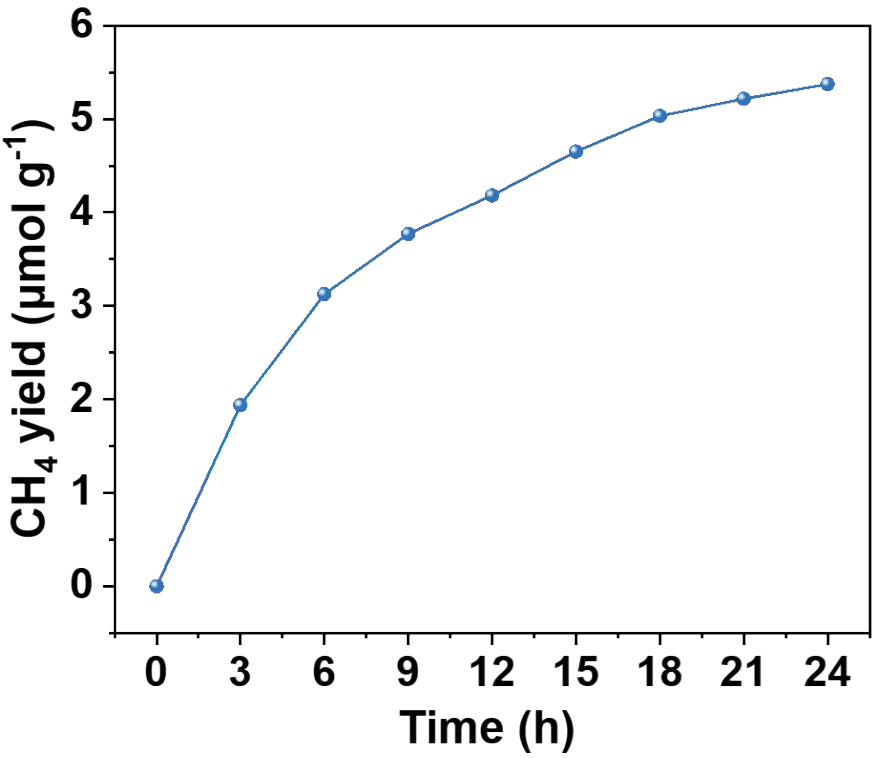


**Fig. S12.** The long-term photocatalytic measurement of La/CuNH under NIR light.

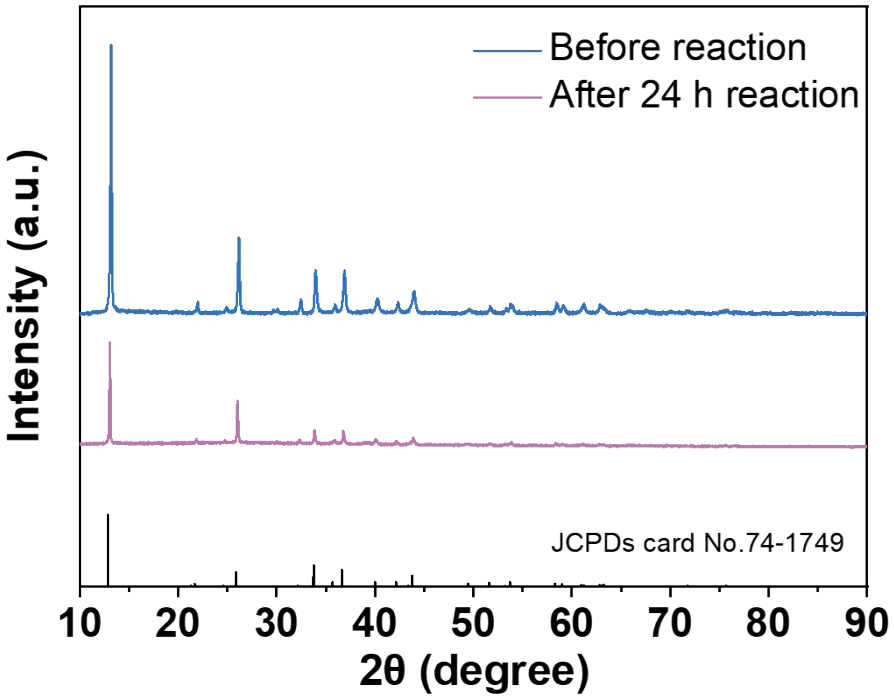


**Fig. S13.** The XRD patterns of La/CuNH before and after 24 h photocatalytic reaction.

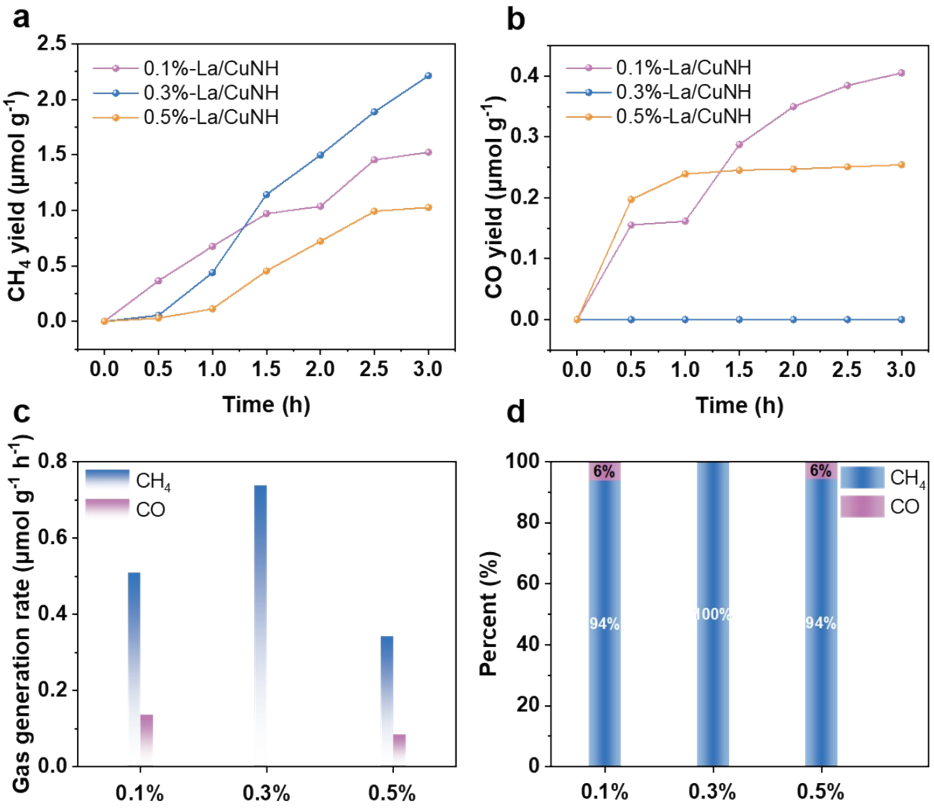


**Fig. S14.** Time-dependent photocatalytic (a) $CH_4$ and (b) CO evolution performance in water vapor under NIR light irradiation (λ≥800 nm) over 0.1%-La/CuNH, 0.3%-La/CuNH, and 0.5%-La/CuNH. (c) The production rates and (d) the product selectivity of 0.1%-La/CuNH, 0.3%-La/CuNH, and 0.5%-La/CuNH.

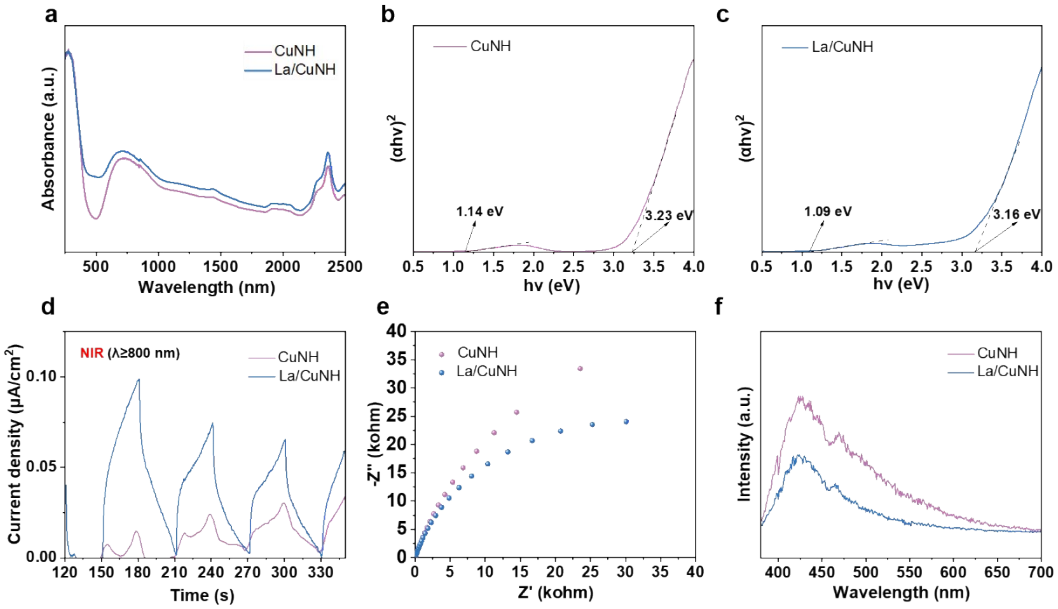


**Fig. S15.** (a) UV-Vis-NIR diffuse reflectance spectra of CuNH and La/CuNH. Tauc plots for (b) CuNH and (c) La/CuNH. (d) Transient photocurrent-time curves and (e) electrochemical impedance spectra (EIS) over CuNH and La/CuNH under NIR irradiation. (f) The steady-state PL spectra of CuNH and La/CuNH.

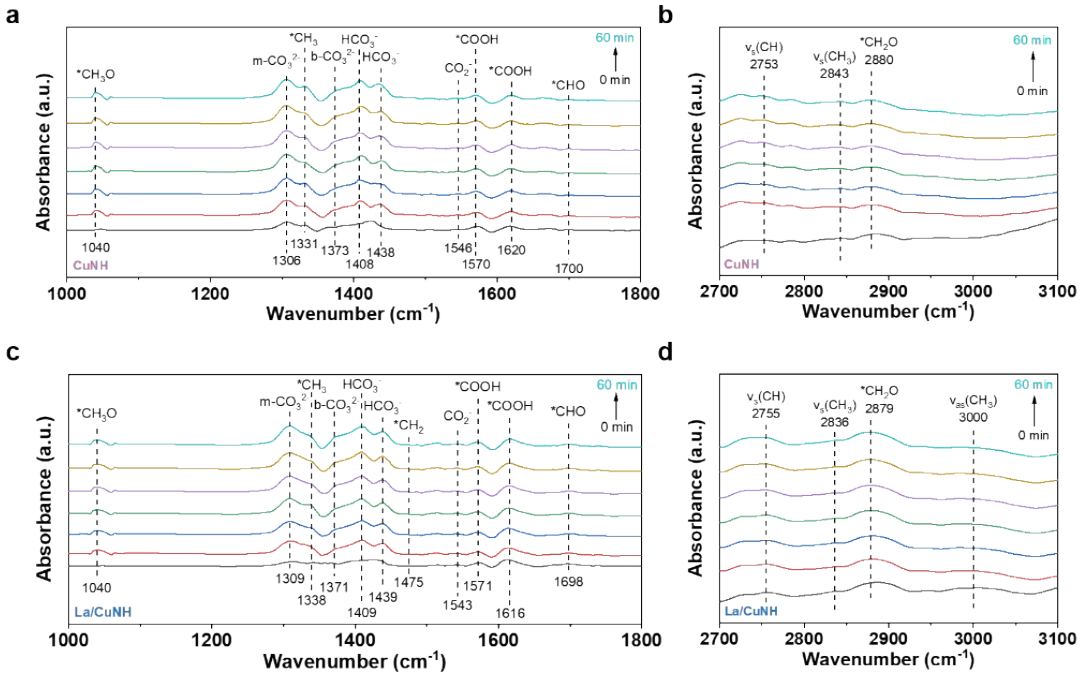


**Fig. S16.** In situ DRIFTS spectra of (a,b) CuNH and (c,d) La/CuNH.

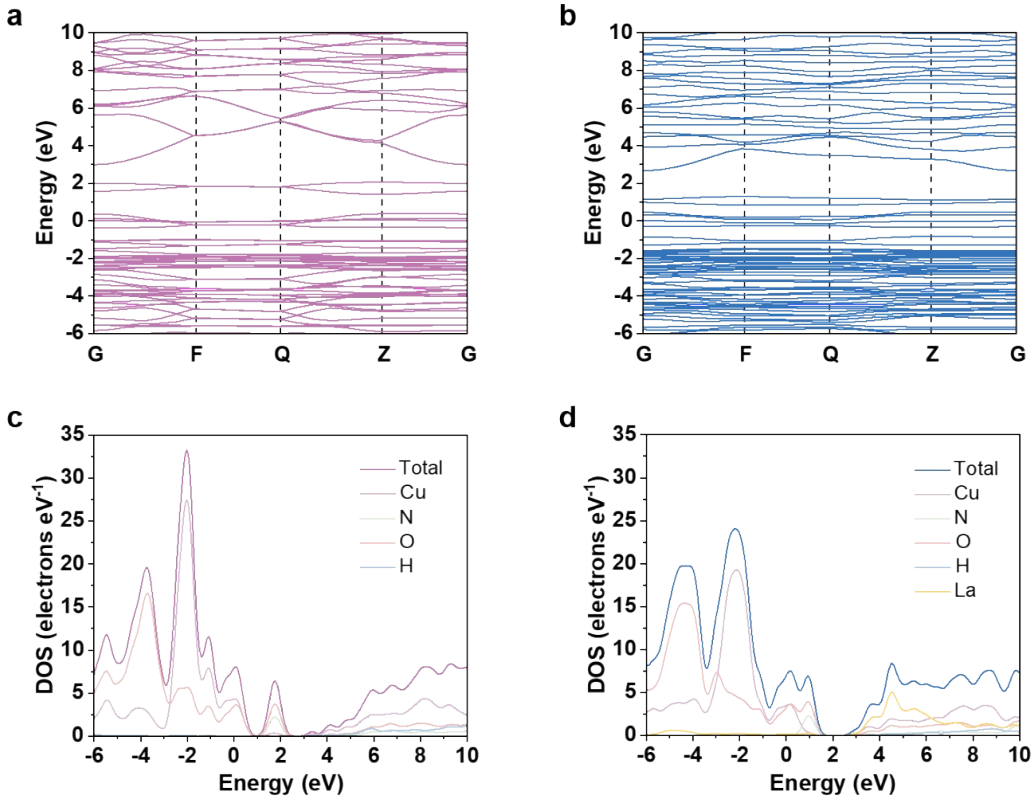


**Fig. S17.** Band structure of (a) CuNH and (b) La/CuNH. Density of states of (c) CuNH and (d) La/CuNH.

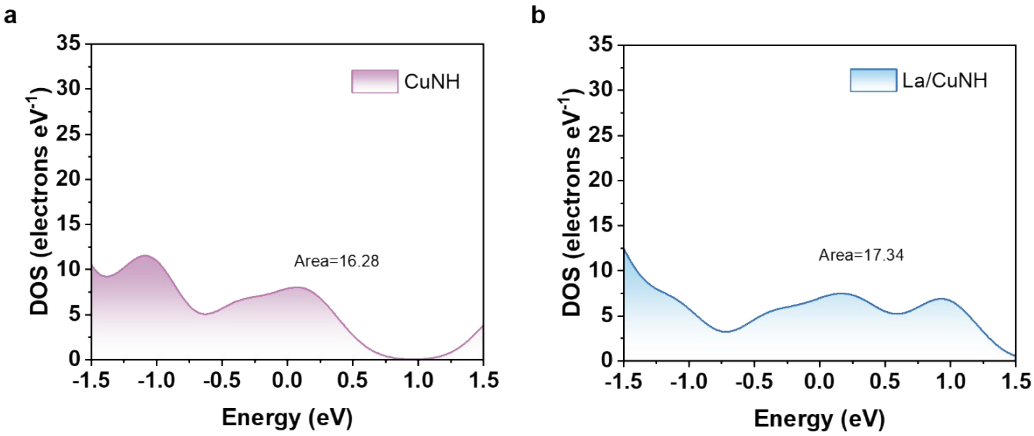


**Fig. S18.** Integrated density of states (DOS) in the range of -1.5 eV to 1.5 eV for (a) CuNH and (b) La/CuNH.

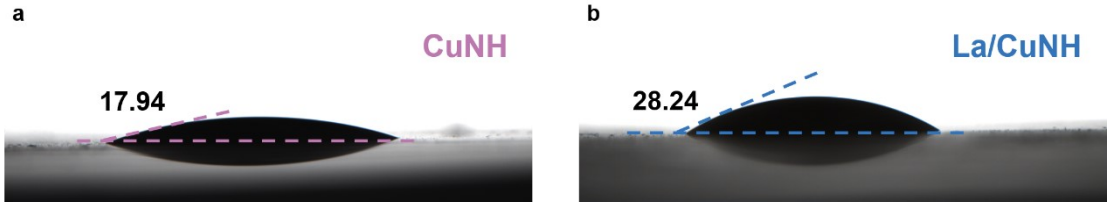


**Fig. S19.** Water contact angles of (a) CuNH and (b) La/CuNH.

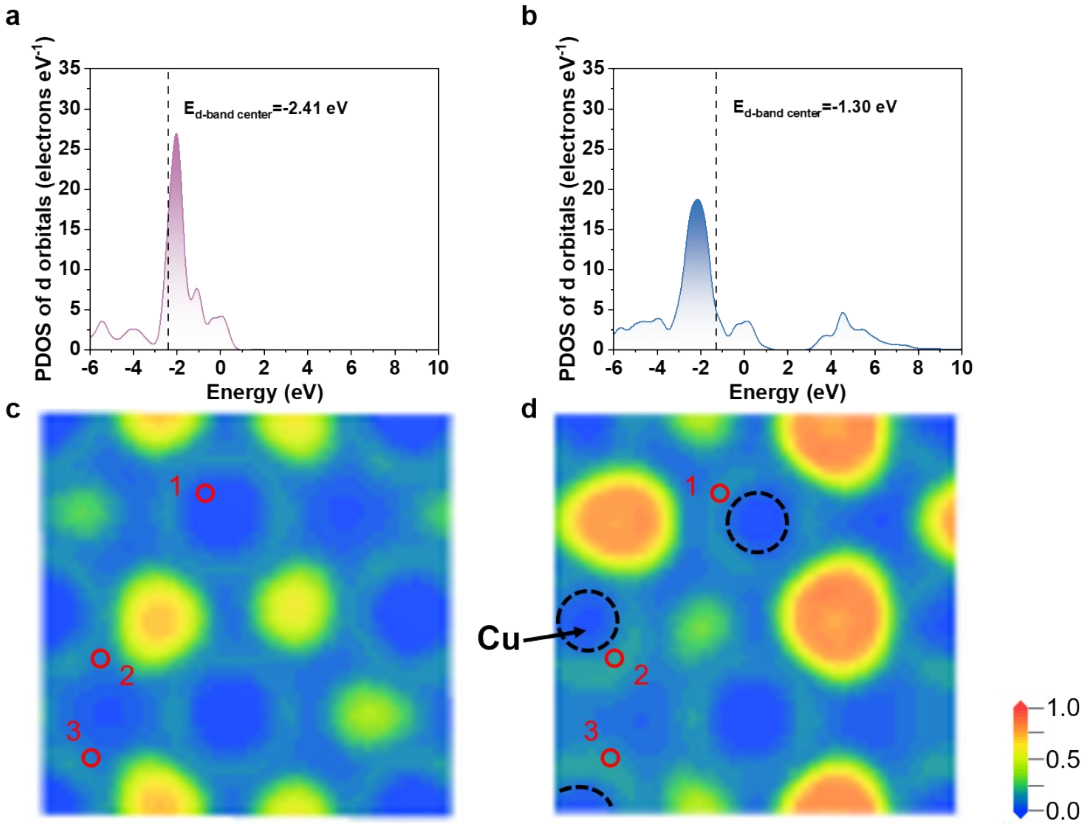


**Fig. S20.** *d*-band center positions of (a) CuNH and (b) La/CuNH. ELF diagrams for (c) CuNH and (d) La/CuNH (The ELF values of regions 1, 2 and 3 are summarized in Table S4).

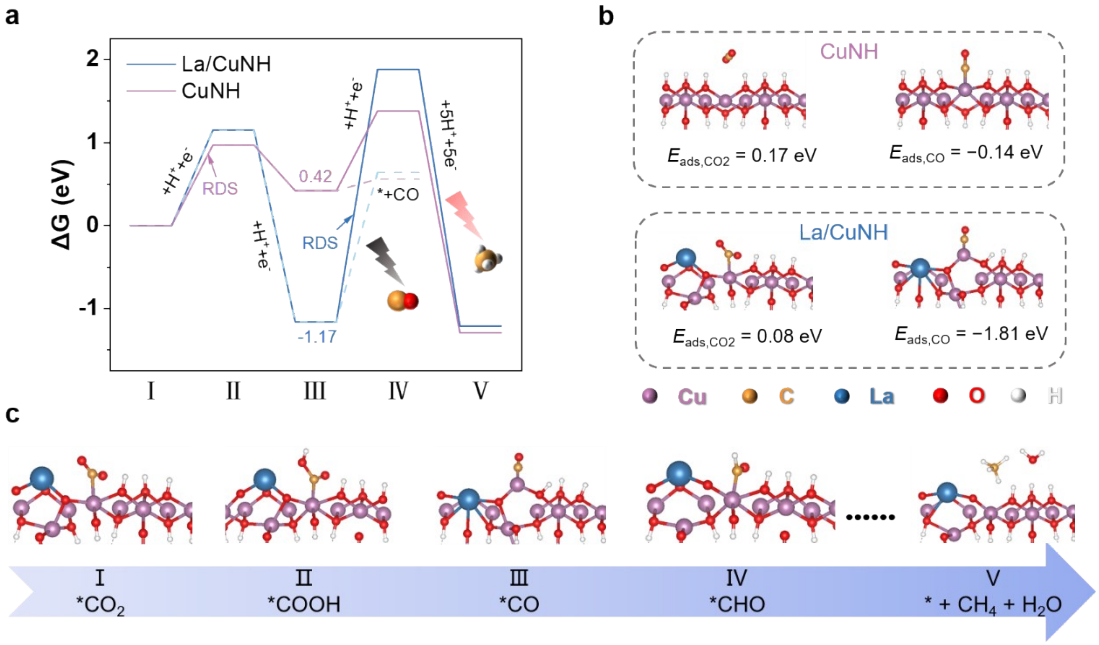


**Fig. S21.** (a) Gibbs free energy diagrams of $CO_2$RR to $CH_4$ and CO over CuNH and La/CuNH. (b) Adsorption energy of $CO_2$ and CO over CuNH and La/CuNH (c) Intermediate structures of La/CuNH during $CO_2$RR under NIR light irradiation. RDS: rate-determining step.

**Table S1.** The details of ICP-MS measurement for La/CuNH.

| Sample | Sample quality $m_0$ (g) | Test element | Test solution element concentration $C_0$ (mg/L) | Sample element content $C_x$ (mg/kg) | Sample element content W (%) |
|---|---|---|---|---|---|
| 0.1%-La/CuNH | 0.1 | La | 0.000413 | 1033 | 0.103% |
| 0.3%-La/CuNH | 0.1 | La | 0.001052 | 2630 | 0.263% |
| 0.5%-La/CuNH | 0.1 | La | 0.001875 | 4688 | 0.469% |

**Table S2.** The molar ratios of La to Cu for La/CuNH.

| Sample | Sample element content W (%) | The molar ratio of La to Cu |
|---|---|---|
| 0.1%-La/CuNH | 0.103% | 0.0009:1 |
| 0.3%-La/CuNH | 0.263% | 0.0023:1 |
| 0.5%-La/CuNH | 0.469% | 0.0041:1 |

**Table S3.** The comparison of $CH_4$ yield and selectivity with other previously reported materials in photocatalytic $CO_2$RR under NIR light.

| Photocatalyst | Light source | Reaction conditions | $CH_4$ Evolution rate (μmol $g^{-1}$ $h^{-1}$) | $CH_4$ Selectivity | Ref. |
|---|---|---|---|---|---|
| $Bi_2WO_6$ with enriched oxygen vacancies | 500 W Xenon arc lamp λ＞700 nm | Gas-solid, water | ~0.05 | N.A. | *Chem. Commun.* **2016**, *52*, 14242-14245. |
| CQDs/UBW | 500 W Xenon arc lamp λ＞700 nm | Gas-solid, water | ~0.05 | N.A. | *Nano Research* **2017**, *10*(5), 1720-1731. |
| 10-BP/WO | 300 W Xe lamp λ＞800 nm | Gas-solid, water | ＜1 | 1% | *Chem. Eng. J.* **2022**, *445*, 136739. |
| UCNPs/ZIS | 300 W Xe lamp λ≥800 nm | Liquid-solid, acetonitrile with TEOA | 0.22 | N.A. | *J. Colloid Interf. Sci.* **2022**, *612*, 782. |
| 1.0% MgPc-BWO | 500 W Xenon arc lamp λ＞700 nm | Gas-solid, water | 0.225 | N.A. | *J. Mater. Chem. C* **2023**, *11*, 705-711. |
| c-CSON | 300 W Xe lamp λ＞800 nm | Gas-solid, water | 4.11 | 15.8% | *Nat. Commun.* **2023**, *14*(1), 4034. |
| bismuthene | 300 W Xe lamp λ≥700 nm | Gas-solid, water | 0.11 | N.A. | *Adv. Mater.* **2024**, *36*, 2312676. |
| $W_{18}O_{49}$@W-Sn NWA | 300 W Xe lamp λ＞700 nm | Gas-solid, water | 3.03 | 98.6% | *Adv. Mater.* **2025**, *37*(4), 2413931. |
| **La/CuNH** | **300 W Xe lamp λ≥800 nm** | **Gas-solid, water** | **0.74** | **~100%** | **This work** |

**Table S4.** The ELF values of CuNH and La/CuNH.

| Region | CuNH | La/CuNH |
|---|---|---|
| 1 | 0.05 | 0.25 |
| 2 | 0.10 | 0.35 |
| 3 | 0.11 | 0.33 |

## Supplementary Reference

[1] Y. Xu, Y. Liu, J. Ye, L. Wang, S. Zhuo and W. Chen, *J. Mater. Chem. C*, 2022, **10**, 6263–6270.